

Supporting Information

Surface Organization of Aqueous MgCl₂ and Application to Atmospheric

Marine Aerosol Chemistry

Nadia N. Casillas-Ituarte¹, Karen M. Callahan², Cheng Y. Tang¹, Xiangke Chen¹, Martina Roeselová³, Douglas J. Tobias² and Heather C. Allen^{1}*

SI Figure Results.

Sum frequency generation (SFG) spectra of aqueous MgCl₂ solutions of 4.7 M at 295 K and 285 K and spectral fits are shown in Fig. S1. While, the hydrogen bonding region below 3550 cm⁻¹ decreases with decreasing temperature, the 3650 cm⁻¹ shoulder and the 3700 cm⁻¹ peak are not affected, confirming that the shoulder at 3650 cm⁻¹ is a dangling OH bond that is not involved in hydrogen bonding with neighboring water molecules (1).

Studies dating to the beginning of vibrational spectroscopic investigation have addressed hydrogen bonding of water in salt solutions (2). Raman and IR spectra of solutions of MgCl₂ (Fig. S2, S3) were obtained to aid in the interpretation of vibrational sum frequency generation spectra. In Fig. S2 (a and b), the parallel-polarized Raman and transmission IR spectra of bulk aqueous MgCl₂ solutions of 0.1 M, 0.3 M, 1.1 M, 2.1 M, 3.1 M and 4.7 M in the OH stretching region are shown. Spectra of neat water are included for comparison. As expected, the free OH peak observed so clearly in the SFG spectra at 3700 cm⁻¹ is not observed in the Raman or IR spectra. Just as in the SFG spectral analysis, the details associated with the spectral assignment of the hydrogen bonding region remains somewhat controversial (3-7), although increasing wavenumber correlates with decreasing hydrogen bonding strength (8-10). The controversy mainly attends to arguments against assigning underlying bands to specific water populations since there are strong intermolecular interactions and coupling that play a role in the shape of the spectra in Raman (6) and IR (11-14). This controversy disallows specific inference to structural details of water coordination and microstructures from vibrational spectra, but this is not addressed in this report. We are mainly interested in comparing the parallel-polarized Raman and IR with the ssp-polarized SFG component band intensities in the hydrogen bonding region to gain insight into the question about the extent that the

hydrogen bonding environment is different at the air/aqueous interface relative to the bulk.

We have also included ATR-IR spectra in the inset of Fig. S2 to illustrate that the change in refractive index alters the spectrum due to the inclusion of the real part of the index. In the past, (9, 15-17) the ATR-IR spectra were used in place of transmission IR because of difficulties with keeping the required short path length of the cell constant. However, we now report a method to circumvent this issue by acquiring the data in transmission mode (where small path length variations are unavoidable) and then normalizing the spectra to the combination band at ~2200 cm⁻¹ since this band is insensitive to addition of the ions. Therefore, we focus on only comparing SFG data to transmission IR as opposed to ATR-IR spectra because of this problem, which becomes particularly significant for the divalent metal cation salts (18-20).

As shown in Fig. S2, the parallel-polarized Raman spectrum of neat water is affected upon addition of MgCl₂. As the concentration is increased, the spectra narrow with the 3200 cm⁻¹ band decreasing in intensity whereas the 3400 cm⁻¹ band increases. The increase in the 3400 cm⁻¹ band is significantly larger than the decrease in the 3200 cm⁻¹ band. We have previously shown (8, 16) that halides strongly perturb the OH stretching region in the Raman spectrum and coined the 3400 cm⁻¹ band as the “solvation shell band” because the polarizability of the water molecules in the solvation shell of a halide become significantly affected by the polarizability of the halide anions (8, 16). Additionally observed, the frequency of the 3400 cm⁻¹ band progressively changes as the concentration is increased. In the transmission IR spectra, an increase in both the 3200 and 3400 cm⁻¹ band is revealed. We also observe a larger enhancement of the 3400 cm⁻¹ band relative to the 3200 cm⁻¹ band consistent with the Raman spectra, although not as dramatic as that which is observed in the Raman. Interesting, but not yet explainable, the 4.7 M MgCl₂ IR spectrum is enhanced more than expected

from the observed enhancement levels of the lower concentration solutions. However, the solution is highly concentrated at 4.7 M MgCl_2 , and a large portion of the water molecules are in primary solvation shells of the Mg^{2+} ions. In our previous work (21), we have shown that Mg^{2+} retains its six solvation shell water molecules in these low water conditions. In the analysis of the intensity trends of the band at $\sim 3400\text{ cm}^{-1}$, the Raman and IR show that the intensity increases with increasing MgCl_2 concentration; but as stated previously, the SFG intensity increases up until 2.1 M and then decreases with further addition of MgCl_2 .

Unpolarized Raman and perpendicular-polarized Raman of the aqueous MgCl_2 solutions of 0.3 M, 1.1 M, 2.1 M, 3.1 M and 4.7 M in the OH stretching region were acquired and are shown in Fig. S3 for reference.

In Fig. S4, comparison plots (left-hand y axis) show the ratio of the 3400 to the $\sim 3250\text{ cm}^{-1}$ band from the SFG ssp, parallel-polarized Raman, and transmission IR spectra. This comparison sheds light on the differences between the surface (SFG) and the bulk solvation environments (Raman and IR). Although we observe only a small variation in the SFG data, the Raman and IR data reveal a substantial increase in this ratio with increasing MgCl_2 molarity, especially in the Raman data. The 3400 cm^{-1} band positions determined by component peak analysis (Table S3, S4) are shown on the right-hand axis of the plots. Opposing trends are observed for the SFG relative to the Raman. Although the Raman and IR frequency trends are not completely consistent with each other, there is an observed red shift from the 4.7 M solution for both. The SFG spectra have a minimum in the peak position plot for the 2.1 M MgCl_2 solution that suggests a different hydrogen bonding structure for the 2.1 M air/solution interface relative to the lower and higher MgCl_2 concentrations.

In Fig. S5, SFG spectra of aqueous MgCl_2 solutions using ssp (top row) and ppp (bottom row) polarization combinations are shown. Spectral analysis was completed to report the orientation angle of the free OH at the surface of the solutions investigated. Orientational analysis of the free OH stretch of neat water has been reported previously (22, 23). Briefly, the ratio of different second order nonlinear polarization tensor elements (χ_{ijk}), in this case ssp ($\chi_{xxz}=\chi_{yyz}$) and ppp (χ_{zzz} , χ_{yyz} , χ_{zyz} , and χ_{zzy}), is related to the mean orientational angle (θ). The orientation angle of the free OH stretch peak is calculated to be $\sim 31^\circ$ which is consistent to the value reported by Gan *et al.* (22).

In Fig. S6, snapshots of the surface and cross-section of the MD simulations as well as density profiles of water O atoms and Mg^{2+} and Cl^- ions are presented. The snapshots were produced using VMD (24). Chloride is present at the interface in all solutions, and its propensity there increases with concentration. 4.8 M MgCl_2 begins to resemble a disordered solid, as evidenced by the organization of chloride at the surface. This was not unexpected given the ability of magnesium to hold onto its first solvation shell and limited availability of water.

Fig. S7 shows water pair interaction energy distributions. The influence of ions on water-water interactions is evident in the histograms of water-water interaction energies computed from the MD simulations and plotted. The peak spanning from around -5 to -2 kcal/mol corresponds to water-water hydrogen bonds, whereas the region around 0 kcal/mol corresponds to non-interacting pairs of water molecules. NaCl and MgCl_2 both reduce the number of water-water hydrogen bonds vs. neat water. In the NaCl solution there is a shoulder on the positive energy side of the main peak at 0 kcal/mol, whereas in the MgCl_2 solutions, there is an additional peak above 2 kcal/mol that grows with increasing MgCl_2 concentration. Evidently, strong ion-water interactions give rise to unfavorable water-water interactions. The existence of these repulsive water-water interactions is clear evidence for change in the water-water hydrogen bonding network in the presence of MgCl_2 , particularly at high concentrations.

In Fig. S8, a plot of free OH number density with respect to Z for each concentration of MgCl_2 and a simulation of pure POL3 water are shown. The Gibbs dividing surface is set to $Z = 0\text{ \AA}$. While the number of free OH oscillators increase with concentration, the orientation of water in the slab becomes more complicated with increasing concentration. The orientation of free OH near the interface remains relatively similar with increasing concentration, but orientation of free OH deeper in the system may cause increased interference with the SFG signal at increasing concentration.

Deconvolution of the SFG ssp spectra from palmitic acid monolayers was carried out and is shown in Fig. S9. These spectra reveal that the CO_2^- modes of palmitic acid with 0.1 M and 1.0 M MgCl_2 subphases have three component peaks, as discussed in the manuscript. The component peaks shown are centered at 1424 cm^{-1} , 1445 cm^{-1} , and 1475 cm^{-1} .

In Fig. S10, radial distribution functions of water around magnesium as a function of position are shown.

While the first and second solvent shells are well defined in all simulations, a shoulder appears outside the second solvation shell in 2.7 M MgCl_2 indicating the emergence of long-range order. Significant restructuring of water around Mg^{2+} is apparent at 4.8 M.

SI Table Results.

The SFG, Raman, and IR spectra were deconvoluted into the component peaks (Table S1, S3, S4, respectively). The fitting parameters included peak position, amplitude, full width half maximum (FWHM) and area. The SFG spectra were fitted with a Lorentzian function whereas in the Raman and IR spectra a Gaussian function was used. In the case of the SFG spectra the phase (+ versus -) was included accordingly to the phase measurements of water obtained from Ji N et al (25). For the SFG spectra the nonresonant terms were kept constant (0.19-0.03i). We also performed extensive sensitivity testing on the magnitude of the nonresonant terms within reasonable values and found that the component peak intensities were reduced with increasing the values; the intensity trends were mostly conserved for the free OH component peaks.

Ab initio calculations were carried out on ion-water clusters using GAUSSIAN03 (26). The initial configurations were taken from MD simulations and optimized at the MP2/6-311++G** level of theory. These coordinates were used as a starting point for a second geometry optimization and vibrational analysis at the MP2/aug-cc-pVDZ level of theory. The results of these calculations are shown in Table S5. Frequencies of water stretches in the first solvation shell of Mg^{2+} are red-shifted when compared to those of water in the first shell of Na^+ .

SI Materials and Methods.

Materials.

A saturated aqueous solution of MgCl_2 was prepared and then filtered through a Whatman Carbon-Cap activated carbon filter to remove organic contaminants. The concentration of the filtered solution was determined by the Mohr method (27). This solution was then diluted in deionized water to the final concentration. To prepare the high concentration solutions (above 3.1 M) the filtered solution was evaporated at 70 °C for several hours to reach the final concentration. The MgCl_2 concentrations used were 0.1 M, 0.3 M, 1.1 M, 2.1 M, 3.1 M and 4.7 M.

Spectroscopy. The SFG spectra shown in the manuscript were obtained with our broadband SFG spectrometer. SFG spectroscopy was utilized because of interface selectivity. It is a second order vibrational spectroscopic technique in which the signal arises from noncentrosymmetric environments, such as at an interface in the dipole approximation. Theoretical details of the SFG process are available in the literature (28-31). The broadband SFG instrument incident angles for the IR and visible beams from the surface normal were 68° and 53°, respectively. The FWHM bandwidth of the infrared beam was typically 200 to 300 cm^{-1} between 3000 and 3800 cm^{-1} . To cover the OH stretching region from 3000 to 3800 cm^{-1} , four spectral regions were used. SFG spectra were normalized to the nonresonant signal from a GaAs crystal for each spectral region. Overlap of the spectral regions as plotted in the figures was completed through a rigorous analysis of the SFG intensity above a threshold value. In some regions, only the top 30% energy maximum spectral region was used in the spectral stitching as determined by additional spectral analysis through varying the central IR peak as determined by the GaAs SFG spectral profile. SFG spectra were obtained under the ssp (s for the SFG, s for the 800 nm, and p for the infrared beam) and ppp polarization combination (at 3700 cm^{-1} , Fig. S5). An average of two replicate spectra is shown in the article, and error bars show ± 1 standard deviation. In the free OH region at 3700 cm^{-1} , the data markers are plotted every 5 data points to improve clarity of the spectra.

Raman spectra were obtained with 100 mW from an unpolarized 532-nm continuous wave laser (Spectra-Physics, Millennia II). The 532 nm beam was focused ~ 1 mm inside a glass vial containing the sample using a 5 mm focusing Raman probe (InPhotonics). The backscattered radiation was collected by the fiber optic probe coupled to the entrance slit of a 500 mm monochromator (Acton Research, SpectroPro SP-500). The Raman scatter was dispersed by a 1200 groove/mm grating blazed at 1 μm and collected on a liquid-nitrogen-cooled CCD camera. The slit width was set to 70 μm . Calibration of the monochromator was completed using the 435.833 nm line from a fluorescent lamp. A naphthalene spectrum was acquired and used to compare its peak positions with literature values (32) as part of the calibration. Raman spectra were acquired with 2 min of exposure time and at $\sim 22 \pm 1$ °C. The average of two Raman spectra is shown.

IR spectra were obtained using a Spectrum Spotlight 300 FT-IR Microscope (Perkin Elmer) in transmission

mode. The salt solutions were placed in-between two CaF₂ windows. A total of 124 scans were acquired for each sample. ATR-FTIR spectra were acquired in a Thermo Nicolet spectrometer (Avantar 370, Thermo Electron Corporation). 128 scans were obtained for each sample.

Computational Methods. Interfacial simulations of aqueous MgCl₂, NaCl, and neat water employed a slab geometry with the unit cell dimensions 30 Å x 30 Å x 100 Å and three-dimensional periodic boundary conditions. The solution slabs were approximately 40 Å thick. The initial coordinates for the interfacial simulations were taken from bulk simulations. The bulk concentrations of the simulations, determined from the composition of the central 14 Å of the slabs, were 1.1 M, 1.9 M, 2.7 M, and 4.8 M. The systems each contained 864 water molecules and 16, 33, 48, and 96 MgCl₂, respectively. The 4.9 M NaCl solution contained 864

water molecules and 96 NaCl. Each simulation was equilibrated for 3 ns, and additional 3 ns were used for data analysis. We employed the polarizable POL3 water model (33), the sodium and chloride model of Perera and Berkowitz (PB) (34), and our previously reported magnesium model (21). The MD trajectories were generated using Sander in the AMBER 8 suite of programs (35) with a modified calculation of induced dipole to avoid polarization catastrophe (36). Particle-mesh Ewald was used to calculate electrostatic interactions (37, 38). The real space part of the Ewald sum and the Lennard-Jones interactions were truncated at 12 Å (37, 38). The time-step was 1 fs and trajectory data were recorded every picosecond. Water bond lengths and angles were constrained using the SHAKE algorithm (39).

References

1. Ma G, Chen X, & Allen HC (2007) Dangling OD confined in a Langmuir monolayer. *J. Am. Chem. Soc.* 129:14053-14057.
2. Franks F Ed (1973) *Water. A comprehensive treatise. Volume 3. Aqueous solutions of simple electrolytes* (Plenum press, New York, NY).
3. Richmond GL (2002) Molecular bonding and interactions at aqueous surfaces as probed by vibrational sum frequency spectroscopy. *Chem. Rev.* 102(8):2693-2724.
4. Shen YR & Ostroverkhov V (2006) Sum-frequency vibrational spectroscopy on water interfaces: polar orientation of water molecules at interfaces. *Chem. Rev.* 106(4):1140-1154.
5. Shultz MJ, Baldelli S, Schnitzer C, & Simonelli D (2002) Aqueous solution/air interfaces probed with sum frequency generation spectroscopy. *J. Phys. Chem. B* 106:5313-5324.
6. Smith JD, *et al.* (2005) Unified description of temperature-dependent hydrogen-bond rearrangements in liquid water. *Proc. Natl. Acad. Sci.* 102(40):14171-14174.
7. Sovago M, *et al.* (2008) Vibrational response of hydrogen-bonded interfacial water is dominated by intramolecular coupling. *Phys. Rev. Lett.* 100(17):173901/1-173901/4.
8. Gopalakrishnan S, Liu D, Allen HC, Kuo M, & Shultz MJ (2006) Vibrational spectroscopic studies of aqueous interfaces: salts, acids, bases, and nanodrops. *Chem. Rev.* 106(4):1155-1175.
9. Levering LM, Sierra-Hernández MR, & Allen HC (2007) Observation of hydronium ions at the air-aqueous acid interface: vibrational spectroscopic studies of aqueous HCl, HBr, and HI. *J. Phys. Chem. C* 111(25):8814-8826.
10. Wang Z, Pang Y, & Dlott DD (2007) Hydrogen-bond disruption by vibrational excitations in water. *J. Phys. Chem. A* 111:3196-3208.
11. Auer BM & Skinner JL (2008) IR and Raman spectra of liquid water: Theory and interpretation. *J. Chem. Phys.* 128:224511/1-224511/12.
12. Auer BM & Skinner JL (2008) Vibrational sum-frequency spectroscopy of the liquid/vapor interface for dilute HOD in D₂O. *J. Chem. Phys.* 129:214705/1-214705/14.
13. Auer BM & Skinner JL (2009) Water: Hydrogen bonding and vibrational spectroscopy, in the bulk liquid and the liquid/vapor interface. *Chem. Phys. Lett.* 470:13-20.
14. Corcelli SA, Lawrence CP, & Skinner JL (2004) Combined electronic structure/molecular dynamics approach for ultrafast infrared spectroscopy of dilute HOD in liquid H₂O and D₂O. *J. Chem. Phys.* 120(17):8107-8117.
15. Gopalakrishnan S, Jungwirth P, Tobias DJ, & Allen HC (2005) Air-liquid interfaces of aqueous solutions containing ammonium and sulfate: spectroscopic and molecular dynamics studies. *J. Phys. Chem. B* 109(18):8861-8872.
16. Liu D, Ma G, Levering LM, & Allen HC (2004) Vibrational spectroscopy of aqueous sodium halide solutions and air-liquid interfaces: observation of increased interfacial depth. *J. Phys. Chem. B* 108(7):2252-2260.

17. Xu M, Spinney R, & Allen HC (2008) Water structure at the air-aqueous interface of divalent cation and nitrate solutions. *J. Phys. Chem. B* 113(13):4102-4110.
18. Max JJ, Blois de S, Veilleux A, & Chapados C (2001) IR spectroscopy of aqueous alkali halides. Factor analysis. *Can. J. Chem.* 79:13-21.
19. Max JJ & Chapados C (1999) Influence of anomalous dispersion on the ATR spectra of aqueous solutions. *Appl. Spectrosc.* 53(9):1045-1053.
20. Max JJ & Chapados C (1999) Interpolation and extrapolation of infrared spectra of binary ionic aqueous solutions. *Appl. Spectrosc.* 53(12):1601-1609.
21. Callahan KM, Casillas-Ituarte NN, Roeselová M, Allen HC, & Tobias DJ (2009) Solvation of magnesium dication: molecular dynamics simulation and vibrational spectroscopic study of magnesium chloride in aqueous solutions. *J. Phys. Chem. B in press.*
22. Gan W, Wu D, Zhang Z, Feng R-R, & Wang H-F (2006) Polarization and experimental configuration analyses of sum frequency generation vibrational spectra, structure, and orientational motion of the air/water interface. *J. Chem. Phys.* 124:114705/1-114705/15.
23. Wei X & Shen YR (2001) Motional effect in surface sum-frequency vibrational spectroscopy. *Phys. Rev. Lett.* 86:4799-4802.
24. Humphrey W, Dalke A, & Schulten K (1996) VMD: visual molecular dynamics. *J. Mol. Graphics* 14(1):33-38.
25. Ji N, Ostroverkhov V, Tian CS, & Shen YR (2008) Characterization of vibrational resonances of water-vapor interfaces by phase-sensitive sum-frequency spectroscopy. *Phys. Rev. Lett.* 096102/1-096102/4.
26. Frisch MJ, *et al.* (2004) Gaussian 03, Revision E.01 (Gaussian, Inc, Wallingford CT).
27. Doughty HW (1924) Mohr's method for determination of silver and halogens in other than neutral solutions. *J. Am. Chem. Soc.* 46(12):2707-2709.
28. Shen YR (1984) *The principles of nonlinear optics* (John Wiley and Sons, New York).
29. Lambert AG & Davies PB (2005) Implementing the theory of sum frequency generation vibrational spectroscopy: a tutorial review. *Appl. Spectrosc. Rev.* 40:103-145.
30. Moad AJ & Simpson GJ (2004) A unified treatment of selection rules and symmetry relations for sum-frequency and second harmonic spectroscopies. *J. Phys. Chem. B* 108(11):3548-3562.
31. Hirose C, Akamatsu N, & Domen K (1992) Formulas for the analysis of the surface SFG spectrum and transformation coefficients of cartesian SFG tensor components. *Appl. Spectrosc.* 42(6):1051-1072.
32. McCreery RL (2000) *Raman Spectroscopy for Chemical Analysis* (Wiley-Interscience, New York).
33. Caldwell JW & Kollman PA (1995) Structure and properties of neat liquids using nonadditive molecular dynamics: water, methanol, and N-methylacetamide. *J. Phys. Chem.* 99(16):6208-6219.
34. Perera L & Berkowitz ML (1991) Many-body effects in molecular dynamics simulations of $\text{Na}^+(\text{H}_2\text{O})_n$ and $\text{Cl}^-(\text{H}_2\text{O})_n$ clusters. *J. Chem. Phys.* 95(3):1954-1963.
35. Case DA, *et al.* (2004) AMBER 8. (University of California, San Francisco).
36. Petersen PB, Saykally RJ, Mucha M, & Jungwirth P (2005) Enhanced concentration of polarizable anions at the liquid water surface: SHG spectroscopy and MD simulations of sodium thiocyanide. *J. Phys. Chem. B* 109(21):10915-10921.
37. Darden T, York D, & Pedersen L (1993) Particle mesh Ewald: an N Log(N) method for Ewald sums in large systems. *J. Chem. Phys.* 98(12):10089-10092.
38. Essmann U, *et al.* (1995) A smooth particle mesh Ewald method. *J. Chem. Phys.* 103(19):8577-8593.
39. Ryckaert JP, Ciccotti G, & Berendsen HJC (1977) Numerical integration of Cartesian equations of motion of a system with constraints: molecular dynamics of *n*-alkanes. *J. Comp. Phys.* 23(3):327-341.

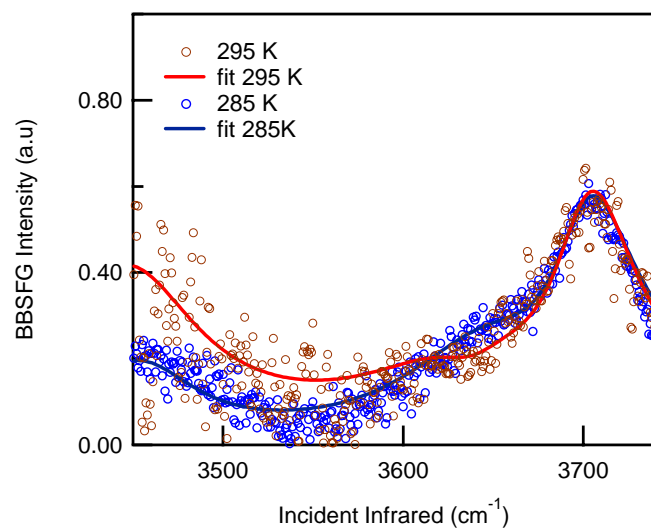


Figure S1. SFG spectra of aqueous 4.7 M MgCl_2 solutions at 295 K and 285 K.

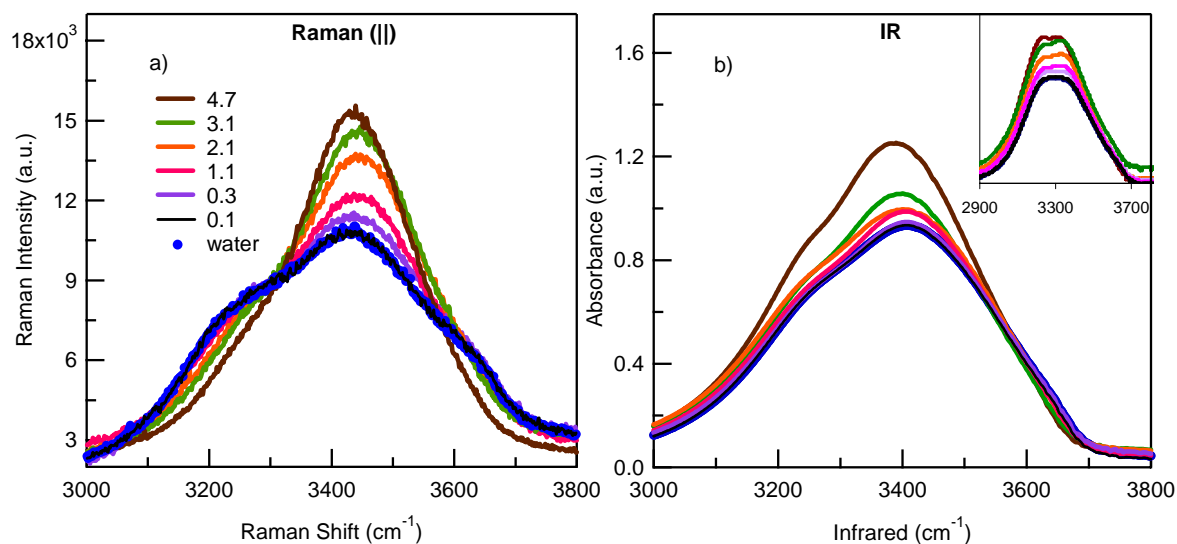


Figure S2. a) Parallel-polarized Raman and b) transmission-infrared spectra of aqueous MgCl_2 solutions of 0.1 M, 0.3 M, 1.1 M, 2.1 M, 3.1 M and 4.7 M in the OH stretching region. Neat water spectra are included for reference. The inset of b) shows the ATR-IR spectra of these solutions.

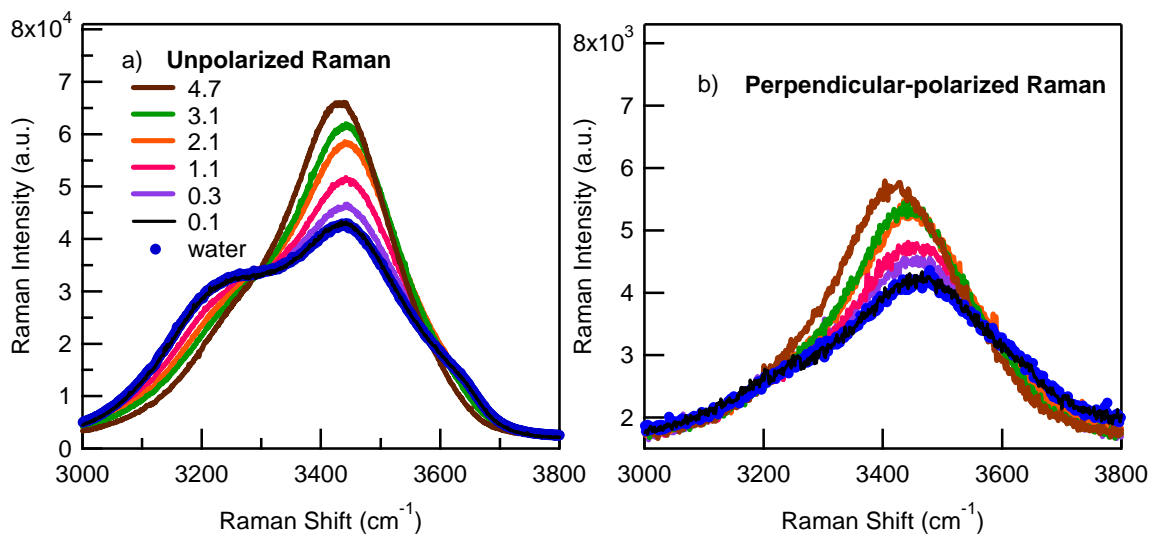


Figure S3. a) Unpolarized Raman and b) perpendicular-polarized Raman spectra of aqueous MgCl_2 solutions of 0.1 M, 0.3 M, 1.1 M, 2.1 M, 3.1 M and 4.7 M in the OH stretching region. Neat water spectra are included for reference.

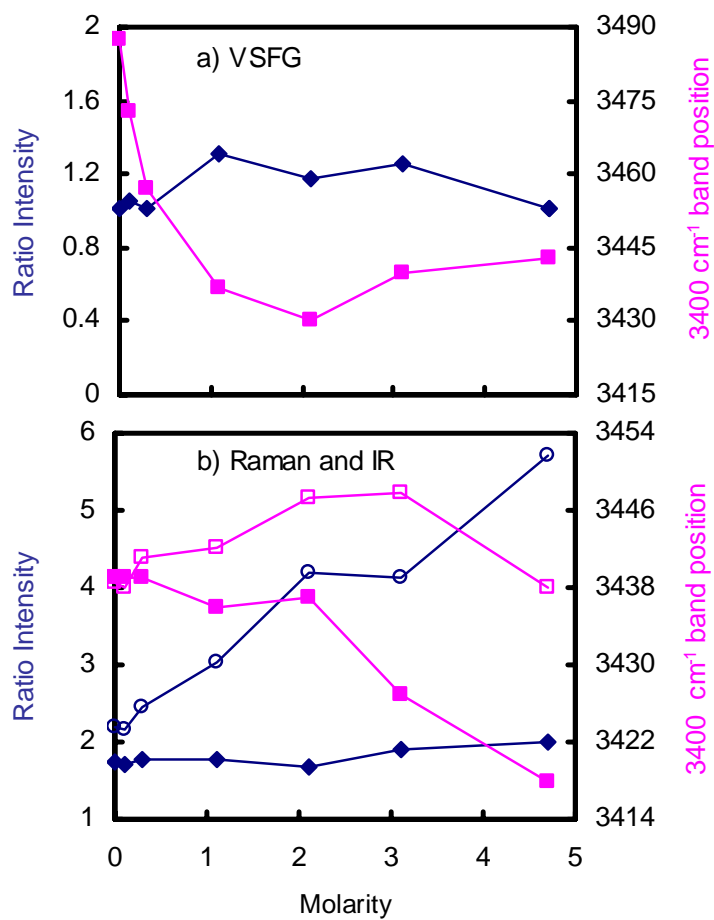


Figure S4. a) SFG, b) parallel-polarized Raman (open symbols), and IR (solid symbols) ratios of the 3400/3250 cm^{-1} bands (dark blue diamonds), and the peak position of the $\sim 3400 \text{ cm}^{-1}$ band (pink squares).

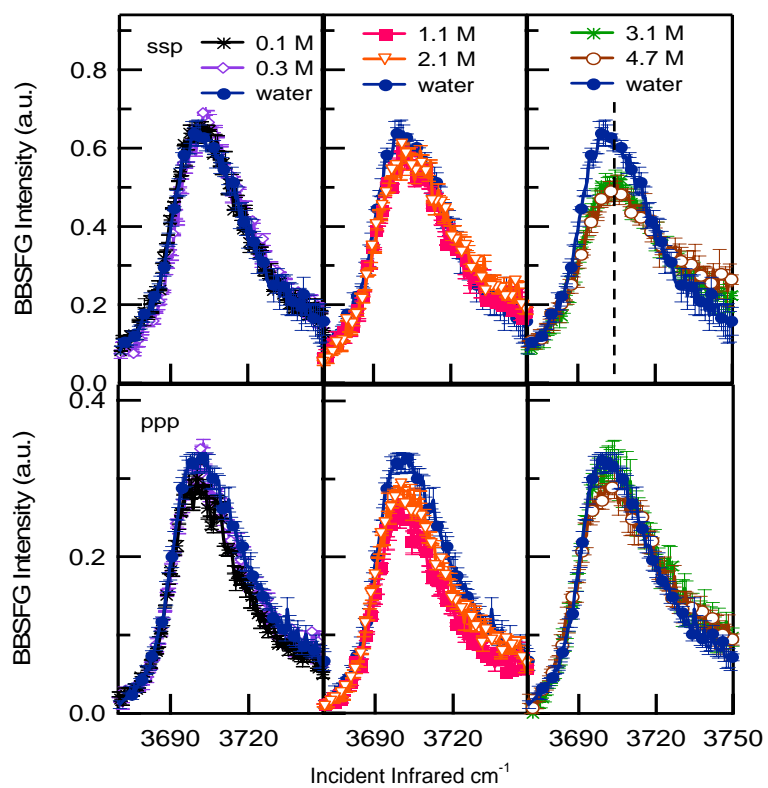


Figure S5. SFG spectra of aqueous MgCl_2 solutions using ssp (top row) and ppp (bottom row) polarization combinations. Neat water spectra are also shown for reference.

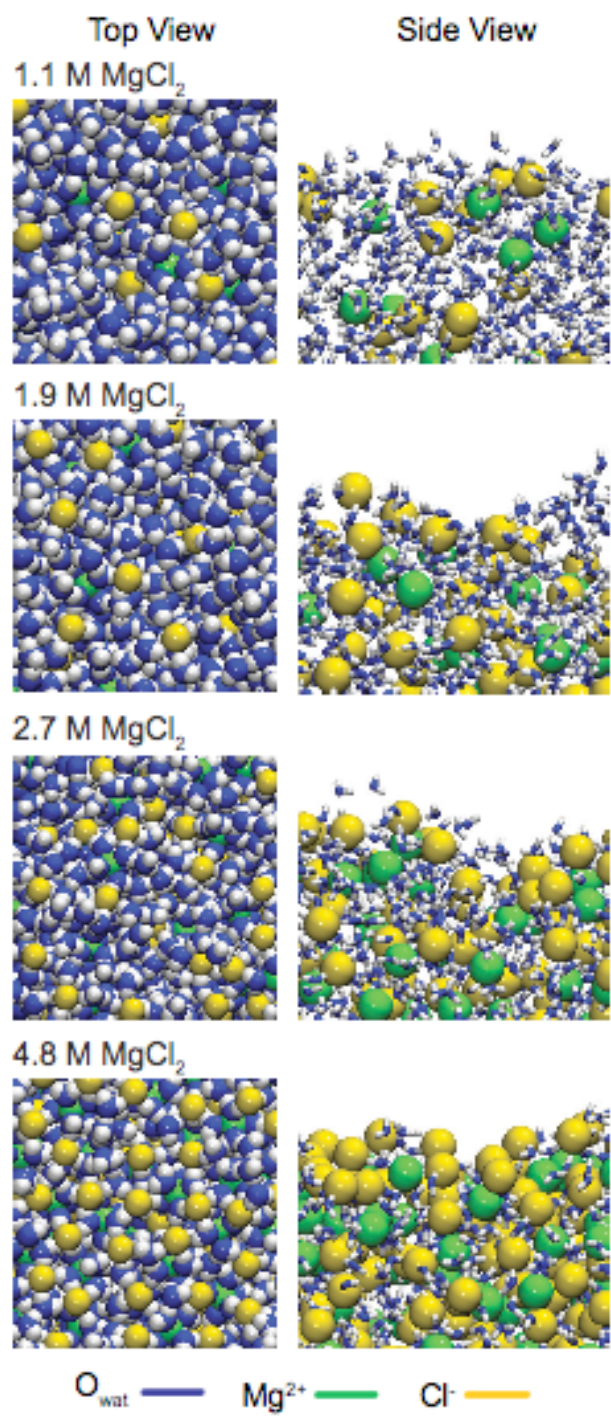


Figure S6. Snapshots of MgCl_2 solutions from MD simulation. In the left column are images of the surface of each system. The right column shows a cross-sectional view of half of each system.

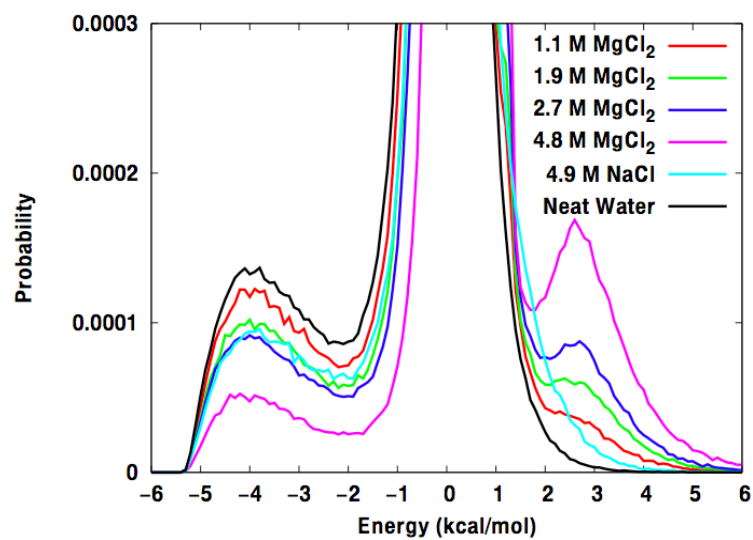


Figure S7. Histograms of water-water interaction energies in simulations of neat water and aqueous solutions of NaCl and MgCl₂.

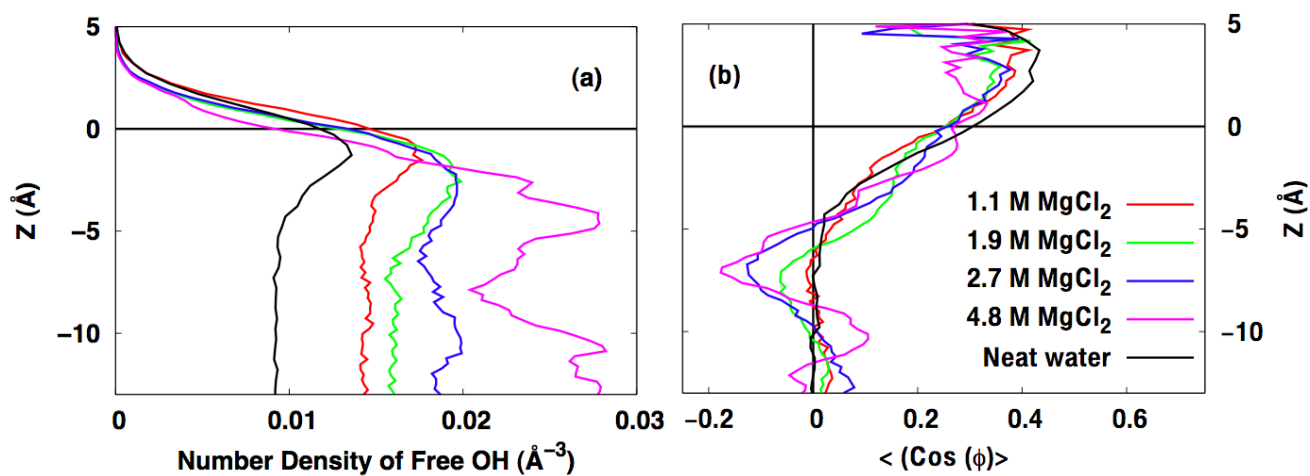


Figure S8. On the left is a plot of free OH number density with respect to Z for each concentration of MgCl_2 as well as for a simulation of pure POL3 water. On the right is the average orientation of the free OH with respect to the Z axis for each of the simulations. The Gibbs dividing surface is set to $Z = 0 \text{ Å}$.

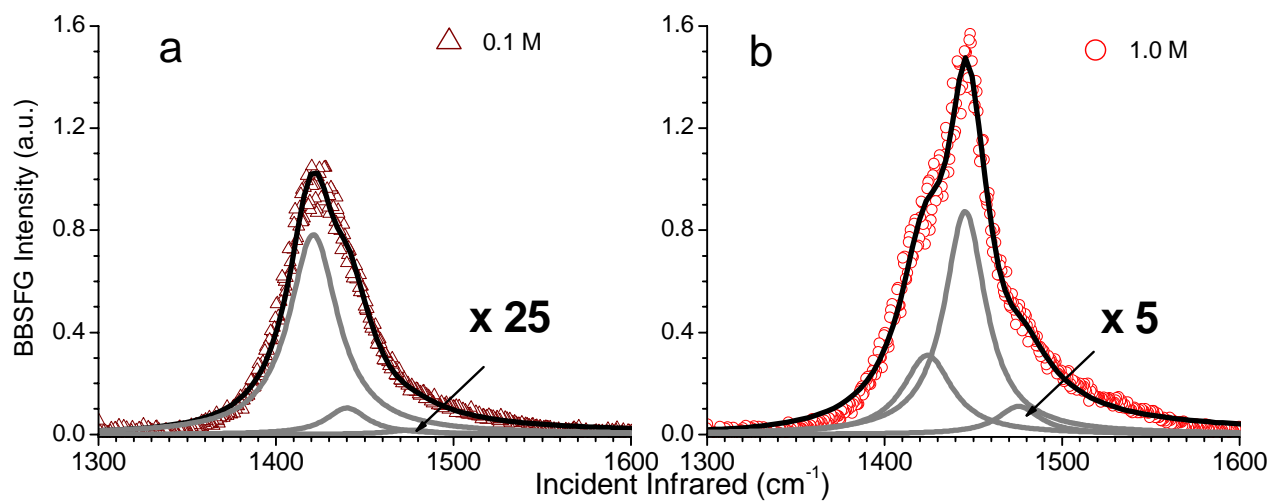


Figure S9. SFG ssp spectra of the CO₂⁻ modes of palmitic acid with a) 0.1 M and b) 1.0 M aqueous MgCl₂ subphases. Component peaks are shown with the overall fits as solid lines that go through the data points.

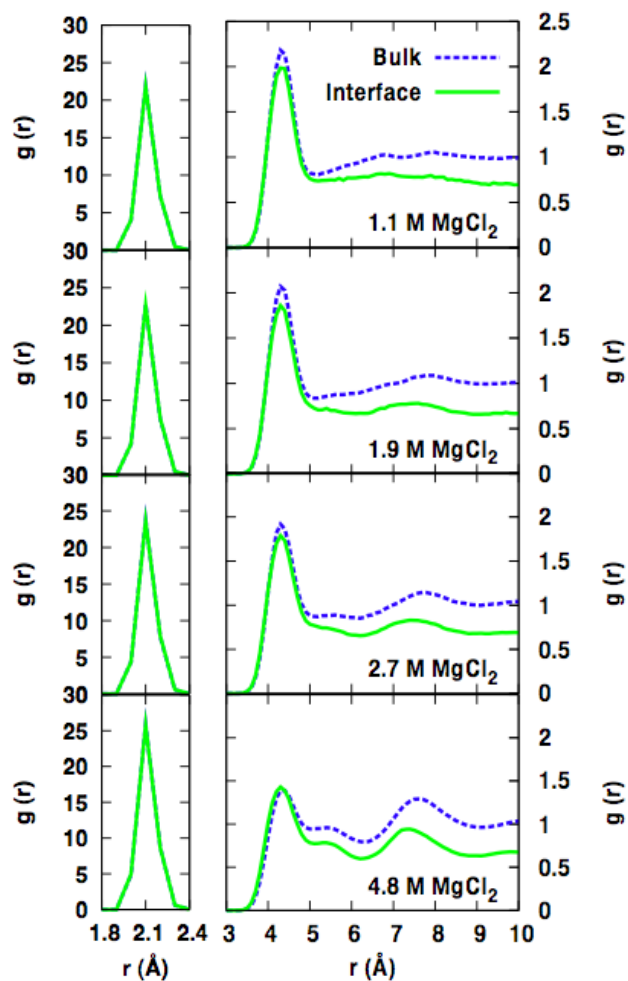


Figure S10. Radial distribution functions of water around magnesium as a function of position. On the left is the region of the first solvation shell, and on the right is the region corresponding to the second solvation shell and beyond. Note the difference in scale. The bulk is defined as the central 14 Å, whereas the interface we define as the first 5 Å below the Gibbs dividing surface.

Table S1. Parameters for the SFG spectral fits of 0.1 M, 0.3 M, 1.1 M, 2.1 M, 3.1 M and 4.7 M MgCl₂ aqueous solutions. Spectral fits were calculated with constant nonresonant terms of 0.019 - 0.03*i*, except the columns denoted by *. Those parameters were obtained with nonresonant terms of 0.35 -0.03*i*.

	Peak position cm ⁻¹	Phase	Amplitude	FWHM	Area (a.u)	Amplitude*	FWHM *	Area (a.u) *
Water	3118	+	48.0	240	41.3			
	3488	-	48.6	200	63.9			
	3645	+	2.0	40	0.6			
	3700	+	13.0	34	30.2			
	3750	+	6.0	110	1.8			
0.1 M MgCl ₂	3125	+	48.3	250	40.2			
	3474	-	50.6	210	65.5			
	3645	+	2.0	40	0.6			
	3701	+	13.1	33.7	31.1			
	3755	+	6.0	110	1.8			
0.3 M MgCl ₂	3128	+	51.3	264	43.3			
	3457	-	52.1	210	69.4			
	3645	+	2.0	40	0.6			
	3702	+	12.5	32.5	29.4			
	3755	+	6.0	110	1.8			
1.1 M MgCl ₂	3160	+	49.21	240	46.5			
	3437	-	64.33	220	100			
	3638	+	1.5	40	0.4			
	3702	+	12.64	35.5	27.3			
	3755	+	8	110	3.2			
2.1 M MgCl ₂	3187	+	62	250	73.1	44	260	34.7
	3430	-	73.3	210	137	60	220	87
	3630	+	1.5	40	0.3	5	60	2.5
	3703	+	13.8	38.4	29.7	12.7	40	24.6
	3755	+	8	80	5.1	1	80	0.07
3.1 M MgCl ₂	3185	+	53.54	230	59.8			
	3440	-	67.33	210	115.6			
	3645	+	0.2	44	0.005			
	3704.4	+	10.5	36.4	18.4			
	3744	+	14.5	110	10.4			
4.7 M MgCl ₂	3174	+	58.6	250	63.7	37	250	25.4
	3449	-	59	182	104.7	47	182	66.5
	3630	+	2	60	0.3	10	80	7.3
	3705	+	12.05	48	18	10.52	43.2	15.4
	3770	+	26	180	18.3	7	180	1.3

Table S2. Concentration of the MgCl₂ aqueous solutions in molarity, mole fraction, and number of water per MgCl₂ and per ion.

Molarity (Moles/L)	Mole fraction (x)	Number of water molecules per MgCl ₂	Number of water molecules per ion (third column/3)*
0.1	0.002	558	186
0.3	0.005	185	62
1.1	0.02	49	16
2.1	0.04	25	8
3.1	0.06	16	5
4.7	0.09	10	3

Table S3. Parameters for the parallel polarized Raman spectral fits of 0.1M, 0.3 M, 1.1 M, 2.1 M, 3.1 M and 4.7 M MgCl₂ aqueous solutions.

	Peak position cm ⁻¹	Amplitude	FWHM	Area (a.u)
Water	3232.2	3535.4	230	188236
	3438.6	7714.8	320	419562
	3630.0	1527.6	180	81378
0.1 M MgCl ₂	3230.7	3576.9	230	190630
	3438.0	7742.6	320	421152
	3630.0	1661.7	180	88558.7
0.3 M MgCl ₂	3232.6	3440.6	230	183081
	3441.0	8414.8	320	457377
	3630.0	1639.7	180	90297
1.1 M MgCl ₂	3219.9	3023.2	230	161957.7
	3442.1	9149.7	320	497011.5
	3630.0	759.2	180	40449.4
2.1 M MgCl ₂	3229.3	2447.5	230	130555.9
	3447.3	10360.6	320	561700.7
	3630.0	428.3	180	22809.4
3.1 M MgCl ₂	3239.3	2748.5	230	158447
	3446.9	11329.7	290	563956
	3630.0	1008.2	180	53730
4.7 M MgCl ₂	3228.3	2157.6	230	115160
	3438	12342.5	280	606778
	3630	450.5	180	28190.7

Table S4. Parameters for the IR spectral fits of 0.1M, 0.3 M, 1.1 M, 2.1 M, 3.1 M and 4.7 M MgCl₂ aqueous solutions.

	Peak position cm ⁻¹	Amplitude	FWHM	Area (a.u)
Water	3239	0.43	338.1	14.9
	3439	0.76	316.8	21.0
	3596	0.10	146	4.8
0.1 M MgCl ₂	3238	0.44	337.3	15.4
	3439	0.77	310.9	22.7
	3596	0.10	141.4	3.1
0.3 M MgCl ₂	3237	0.43	342.7	14.8
	3439	0.76	314	22.5
	3593	0.10	140.3	2.9
1.1 M MgCl ₂	3234.7	0.44	357.8	15.5
	3436.6	0.79	313.8	23.3
	3589	0.08	135.8	2.6
2.1 M MgCl ₂	3234.3	0.47	348	16.5
	3436.7	0.79	312.3	23.3
	3579.7	0.08	120	2.4
3.1 M MgCl ₂	3233	0.44	346	15.3
	3427	0.83	304	24.7
	3582	0.08	121.1	2.4
4.7 M MgCl ₂	3233	0.50	350	18.1
	3418.7	1.0	308	29.6
	3576	0.097	118.1	2.8

Table S5. Harmonic Frequencies and Infrared Intensities of OH and OD stretches of HOD and H₂O in HOD-D₂O-ion clusters and H₂O-D₂O-ion clusters^a ^aComputed at the MP2/aug-cc-pVDZ level of theory.

Cluster	IR Frequency (cm ⁻¹)	IR Intensity (km·mol ⁻¹)	Assignment
Mg ²⁺ ·H ₂ O·(D ₂ O) ₅	3762	105	Sym. stretch
	3867	186	Asym. stretch
Na ⁺ ·H ₂ O·(D ₂ O) ₅	3764	44	Sym. stretch
	3896	141	Asym. Stretch
Mg ²⁺ ·HOD·(D ₂ O) ₅	2772	77	OD stretch
	3816	151	OH stretch
Na ⁺ ·HOD·(D ₂ O) ₅	2758	65	OD stretch
	3865	67	OH stretch